Effect of angular momentum conservation on hydrodynamic simulations of colloids

Mingcheng Yang,[1,2,*] Mario Theers,[3] Jinglei Hu,[2] Gerhard Gompper,[2,3] Roland G. Winkler,[3] and Marisol Ripoll[2,†]

[1]*Beijing National Laboratory for Condensed Matter Physics and Key Laboratory of Soft Matter Physics, Institute of Physics, Chinese Academy of Sciences, Beijing 100190, China*

[2]*Theoretical Soft-Matter and Biophysics, Institute of Complex Systems, Forschungszentrum Jülich, 52425 Jülich, Germany*

[3]*Theoretical Soft-Matter and Biophysics, Institute for Advanced Simulation, Forschungszentrum Jülich, 52425 Jülich, Germany*

(Received 6 February 2015; published 2 July 2015)

In contrast to most real fluids, angular momentum is not a locally conserved quantity in some mesoscopic simulation methods. Here we quantify the importance of this conservation in the flow fields associated with different colloidal systems. The flow field is analytically calculated with and without angular momentum conservation for the multiparticle collision dynamics (MPC) method, and simulations are performed to verify the predictions. The flow field generated around a colloidal particle moving under an external force with slip boundary conditions depends on the conservation of angular momentum, and the amplitude of the friction force is substantially affected. Interestingly, no dependence on the angular momentum conservation is found for the flow fields generated around colloids under the influence of phoretic forces. Moreover, circular Couette flow between a no-slip and a slip cylinder is investigated, which allows us to validate one of the two existing expressions for the MPC stress tensor.

DOI: 10.1103/PhysRevE.92.013301 PACS number(s): 02.70.−c, 47.11.−j, 47.57.J−

I. INTRODUCTION

To effectively investigate the dynamical behavior of mesoscale objects, such as colloids, by computer simulations, the application of a coarse-grained solvent has been shown to be of paramount importance. This is due to the advantageous bridging of the enormous length- and time-scale gap between the solvent and solute degrees of freedom [1,2]. The most prominent coarse-grained mesoscale approaches developed during the last decades are the lattice Boltzmann method [3], direct simulation Monte Carlo [4,5], dissipative particle dynamics (DPD) [6–8], and the multiparticle collision dynamics (MPC) approach [9–11]. In spite of disregarding the microscopic details of real solvents, these techniques successfully capture most relevant solvent features, such as hydrodynamic interactions, thermal fluctuations, or heat conduction, and thus provide access to length and time scales, where most of the relevant phenomena in soft matter systems take place.

Conservation laws play a key role in the construction of mesoscopic approaches. Specifically, local conservation of mass and translational momentum guarantee the correct hydrodynamic behavior [9,12], and local energy conservation properly reproduces heat conduction processes [13–15]. In contrast, local angular momentum conservation (AMC) has a less obvious effect, and there are simulation approaches in which AMC is violated. This is the case in certain versions of the MPC approach, like the frequently used stochastic rotation dynamics (MPC-SRD) algorithm, an extension of DPD with tangential friction forces [16], and in the smoothed dissipative particle dynamics (SDPD) approach [17]. Note that an angular momentum conserving SDPD variant is proposed in Ref. [18].

As is well known, the violation of AMC does not affect the generic form of the hydrodynamic equations [19–22]. However, the fluid stress tensor is no longer symmetric [19,23–26], which affects the propagation of sound but is unimportant for the evolution of vorticity of a bulk fluid. A detailed simulation study by Götze *et al.* [26] indicates that the absence of AMC leads to a nonphysical contribution to the torque in the case of circular Couette flow, or even an incorrect velocity field in the case of rotating inhomogeneous solutions. Here the coupling of the boundary condition and stress tensor leads to additional effects, which are not present for AMC simulations with a symmetric stress tensor. The importance of AMC could be intuitively expected for systems with intrinsic rotations [26–29] but seems irrelevant for nonrotating systems. Hence, MPC has been widely employed in simulations of colloidal suspensions [14,15,22,30–41], without investigation of the relevance of AMC on their transport properties.

The intimate coupling between the fluid stress tensor and the boundary condition occurs for slip boundary conditions, where the stress tensor explicitly appears [42]. Thus, the lack of AMC may produce specific dynamical effects for colloidal particles with slip boundaries. These conditions are, on the one hand, much easier to implement in simulations than the no-slip ones [31,40], and partial slip is often more appropriate for many experimental situations. Moreover, a slip boundary can be necessary to produce significant observable effects, e.g., in simulations of colloidal phoresis [14,15] or synthetic active colloids [33,36,38,41,43,44]. Therefore, an obvious question is how important local AMC is in the simulation of colloids, or equivalently, in which situations AMC is negligible. To answer these questions is not only of theoretical interest, but also essential for a proper design of simulation models and the interpretation of simulation results.

In this paper, we investigate analytically and by MPC simulations how the absence or presence of AMC influences the flow field around a colloidal sphere with slip boundary and how it affects its frictional properties. The flow field is calculated for three typical situations: (1) a particle moving under an external force like gravity, (2) a particle driven by a phoretic force (internal force), and (3) a fixed particle in

*mcyang@iphy.ac.cn
†m.ripoll@fz-juelich.de

the presence of a phoretic force. As a result, no effect due to the absence of AMC is observed for phoretic particles. However, significant quantitative differences are found in the case of a particle moving under an external force, where, most importantly, the amplitude of the friction coefficient is affected. Moreover, we investigate the Couette flow between two cylinders with slip and no-slip boundary conditions. The emerging flow profile strongly depends on the absence or presence of AMC, as well as on the underlying stress tensor.

The paper is organized as follows. In Sec. II, the multiparticle collision dynamics simulation approach is described and boundary conditions are specified. In Sec. III, the stress tensors are discussed and a link to the Stokes equation is established. In Sec. IV, the analytical solutions of the Stokes equation are presented with and without AMC for a spherical colloidal particle moving in an external field and under the influence of a phoretic field, for which both a fixed and a moving particle are considered. The various simulation results are discussed in Sec. IV; in particular, the effect of AMC on the friction coefficient is analyzed. In order to clearly distinguish the two existing versions of nonangular momentum-conserving MPC stress tensors, Sec. V investigates the velocity field for a circular Couette flow.

II. MULTIPARTICLE COLLISION DYNAMICS

A. Algorithm

The fluid is represented by N point particles, with the mass m, position $\boldsymbol{r}_i$, and velocity $\boldsymbol{v}_i$ of particle i, $i \in \{1,\ldots,N\}$. The particle dynamics is time-discretized and consists of a streaming and a collision step. In the streaming step, the fluid particles move ballistically, hence,

$$\boldsymbol{r}_i(t+h) = \boldsymbol{r}_i(t) + h\boldsymbol{v}_i(t), \tag{1}$$

where h is the collision time. For the collision step the simulation box is divided into cubic collision cells of length l_c in which multiparticle collisions take place. These are described by the velocity update

$$\boldsymbol{v}_i(t+h) = \boldsymbol{v}_{\mathrm{cm}}(t) + \boldsymbol{\Omega}[\boldsymbol{v}_i(t) - \boldsymbol{v}_{\mathrm{cm}}(t)], \tag{2}$$

where $\boldsymbol{v}_{\mathrm{cm}}$ is the center-of-mass velocity of each collision cell and $\boldsymbol{\Omega}$ is the collision operator [45]. In order to guarantee Galilean invariance, the grid of collision cells is randomly shifted at each time step [46].

Implementations of MPC differ in the collision operator $\boldsymbol{\Omega}$. Due to the conservation of mass and linear momentum all implementations of MPC obey the Navier-Stokes equations on large length and time scales [9]. In the most standard implementation, here referred to as MPC-SRD, the velocities of the particles relative to the collision cell center-of-mass velocity are rotated by a fixed angle α around a randomly oriented axis [9–11,30]. In this case, as can easily be proven, energy is locally conserved, but not angular momentum. In an alternative implementation, known as MPC-AT, the velocities of the particles relative to the collision cell center-of-mass velocity are randomly chosen from a Maxwell-Boltzmann distribution [45,47]. MPC-AT does not locally conserve energy, nor angular momentum, but it effectively ensures a constant temperature T in the presence of external driving, such as confinement, or applied forces. In order to account for angular momentum conservation, an additional term has to be added in the velocity update in Eq. (2), which therefore warrants a symmetric stress tensor. We distinguish between MPC-SRD-a and MPC-SRD+a as well as MPC-AT-a and MPC-AT+a, where +a indicates AMC and -a the lack thereof [45].

In simulations, lengths are measured in units of the collision cell size l_c and time in units of $\sqrt{ml_c^2/k_BT}$. This corresponds to setting $m = 1$, $l_c = 1$, and $k_BT = 1$, where k_B is the Boltzmann constant and T the temperature.

B. Solid boundaries

The interactions of solvent particles with solid boundaries strongly depend on the interface properties. Two of the most common boundary conditions are slip and no-slip boundaries. In MPC, such boundaries can be implemented similarly as in other mesoscopic simulation approaches. Slip boundary conditions at walls are realized by specular reflection of the MPC particles at the boundary, i.e., $v_n \to -v_n$, where $v_n = \boldsymbol{n}\cdot\boldsymbol{v}$ and $\boldsymbol{n}$ is the boundary normal vector at the point of collision. Thus, the momentum parallel to the interface is conserved. Alternatively, central potentials (like a Lennard-Jones potential) between, e.g., a planar solid boundary and the fluid particles leads to slip boundary conditions. For no-slip boundary conditions, the bounce-back rule is applied at the boundary in the co-moving frame, i.e., $\boldsymbol{v} \to -\boldsymbol{v}$ [10,11]. By the random shift of the collision lattice, cells intersected by walls are only partially filled. Here additional virtual wall particles are introduced to reestablish no-slip boundary conditions [48–50]. The simulation of colloids follows the same principles. In the case of no-slip boundary conditions, special considerations have to be made in order to account for curved, moving surfaces, which can eventually describe a rotational motion [26,40,41]. In this work, we concentrate on slip boundary conditions and employ specular reflections.

III. HYDRODYNAMICS

The hydrodynamic properties of the MPC fluid are excellently described by the linearized Navier-Stokes equation

$$\varrho\frac{\partial}{\partial t}\boldsymbol{v}(\boldsymbol{r},t) = \nabla\cdot\boldsymbol{\sigma}(\boldsymbol{r},t) \tag{3}$$

on sufficiently large length and time scales [9,10,19,25,51,52]. Here ϱ denotes the average fluid mass density, $\boldsymbol{v}(\boldsymbol{r},t)$ the fluid flow field at $\boldsymbol{r}$ and time t, and $\boldsymbol{\sigma}(\boldsymbol{r},t)$ the stress tensor.

A. Stress tensor

The stress tensor for a MPC fluid has been addressed in, e.g., Refs. [19,20,25,26]. For no-slip boundary conditions, the flow properties are determined by the requirement that the fluid velocity is zero at the surface; i.e., the boundary condition is independent of the stress tensor, and, in turn, the solution of the Navier-Stokes equation (3) is independent of the explicit stress tensor. However, in the presence of (partial) slip, the boundary condition includes the stress tensor explicitly, and the solution of the Navier-Stokes equation depends on the stress tensor. Hence, a different choice of the tensor will be reflected in the resulting flow field.

In general, the stress tensor for MPC can be expressed as

$$\boldsymbol{\sigma} = -P\boldsymbol{I} + \hat{\eta}\nabla\boldsymbol{v}^T + \eta(\nabla\boldsymbol{v}^T)^T + \bar{\eta}(\nabla\cdot\boldsymbol{v})\boldsymbol{I}, \quad (4)$$

where $\boldsymbol{I}$ is the identity matrix, P the local pressure, and $\eta = \eta^c + \eta^k$ the fluid viscosity, which is the sum of collisional and kinetic contributions. The trace of the stress tensor is related with the bulk viscosity, $\eta_V = (\hat{\eta} + \eta + 3\bar{\eta})/3$. The suggested stress tensors for MPC-SRD-a differ in their values for $\hat{\eta}$ and $\bar{\eta}$. A Green-Kubo approach is used by Ihle, Tüzel, and Kroll in Ref. [19], which cannot uniquely determine the stress tensor. These authors have derived and presented various valuable results for MPC-a fluid transport coefficients in Refs. [19,20]. In Ref. [20], it is suggested that the bulk viscosity of MPC-a should be zero, from which it can be concluded that

$$\hat{\eta} = \eta^k + \eta^c/2, \quad \bar{\eta} = -2\eta^k/3 - \eta^c/2. \quad (5)$$

Pooley and Yeomans [25] calculated the stress tensor directly without any ambiguity with

$$\hat{\eta} = \eta^k, \quad \bar{\eta} = -2\eta^k/3. \quad (6)$$

Note that these values imply a nonzero bulk viscosity. In Ref. [54], Ihle derived the Pooley and Yeomans stress tensor by a Chapman-Enskog expansion. For an angular-momentum conserving fluid, the stress tensor is symmetric, hence, $\hat{\eta} = \eta$. Also in this case, the bulk viscosity is nonzero as discussed in Ref. [53]. The presence of η_V does not directly affect the results discussed in this article, since we focus on the incompressible limit. In the kinetic or particle regime where the fluid has a gaslike behavior and $\eta^k \gg \eta^c$, the effect of AMC is negligible and the two expressions of the stress tensor just converge to the symmetric form.

The explicit dependence of the viscosities η^k and η^c on the MPC parameters, i.e., collision step size, rotation angle, and particle density, has been determined by various methods for MPC-a [19,25,30,45,46,50,55] and MPC+a variants [45], and it is now well established.

B. Stokes limit

Analytical expressions for hydrodynamic flows are obtained as solution of the Navier-Stokes equations with adequate boundary conditions. In this article, we focus on steady state systems with small Reynolds and Mach numbers, such that time derivatives and nonlinear terms can be neglected. The stationary velocity field obeys then the Stokes equations

$$\nabla\cdot\boldsymbol{\sigma} = 0, \quad \nabla\cdot\boldsymbol{v} = 0, \quad (7)$$

and insertion of the stress tensor (4) yields

$$-\nabla P + \eta\Delta\boldsymbol{v} = 0. \quad (8)$$

This equation contains just η as viscosity value, such that it is identical for both mentioned stress tensors. As discussed above, a dependence on AMC appears due to the boundary conditions.

IV. SPHERICAL COLLOID

The Stokes equations (7) and (8) can easily be solved for a spherical colloidal particle, either moving with velocity $\boldsymbol{u}$ or when a constant external force $\boldsymbol{F}$ is applied. The general solution of the flow field in both cases can be written as [42]

$$\boldsymbol{v}(\boldsymbol{r}) = -\frac{a}{r}(\boldsymbol{I} + \hat{\boldsymbol{r}}\hat{\boldsymbol{r}}^T)\cdot\boldsymbol{g} - \frac{b}{r^3}(\boldsymbol{I} - 3\hat{\boldsymbol{r}}\hat{\boldsymbol{r}}^T)\cdot\boldsymbol{g} + c\boldsymbol{g}, \quad (9)$$

where $\boldsymbol{r}$ is the position vector from the particle center, $\hat{\boldsymbol{r}} = \boldsymbol{r}/|\boldsymbol{r}|$, $\boldsymbol{g}$ refers to either $\boldsymbol{u}$ or $\boldsymbol{F}$, depending on the case of study, and $\hat{\boldsymbol{r}}\hat{\boldsymbol{r}}^T$ denotes the tensorial product. The local pressure can be expressed as

$$P = 2a\eta\boldsymbol{g}\cdot\nabla\left(\frac{1}{r}\right) + P_0, \quad (10)$$

with P_0 the pressure at infinity. The first term in Eq. (9) is a Stokeslet term, which decays with the inverse of the distance r and is therefore long-ranged. The second term is a source-dipole term which shows a faster decay with the inverse of the distance cubed. The third term is a constant, which is given by the flow velocity at infinity. The coefficients a,b, and c in Eqs. (9) and (10) are determined by the hydrodynamic boundary conditions [42] and are therefore different for different boundary conditions.

Due to symmetry, it is convenient to employ spherical coordinates with the polar axis along $\boldsymbol{g}$, i.e., $\boldsymbol{v} = v_r\hat{\boldsymbol{r}} + v_\theta\hat{\boldsymbol{\theta}} + v_\phi\hat{\boldsymbol{\phi}}$, with the unit vectors $\hat{\boldsymbol{r}}$, $\hat{\boldsymbol{\theta}}$, and $\hat{\boldsymbol{\phi}}$; hence, the solution of Eq. (9) can be written as

$$v_r(\boldsymbol{r}) = g\cos\theta\left(-\frac{2a}{r} + \frac{2b}{r^3} + c\right), \quad (11)$$

$$v_\theta(\boldsymbol{r}) = -g\sin\theta\left(-\frac{a}{r} - \frac{b}{r^3} + c\right). \quad (12)$$

A vanishing velocity field at infinity implies $c = 0$. Note that in spherical coordinates the gradient is

$$\nabla = \hat{\boldsymbol{r}}\frac{\partial}{\partial r} + \hat{\boldsymbol{\theta}}\frac{1}{r}\frac{\partial}{\partial\theta} + \hat{\boldsymbol{\phi}}\frac{1}{r\sin\theta}\frac{\partial}{\partial\phi}, \quad (13)$$

and thus

$$\boldsymbol{g}\cdot\nabla\left(\frac{1}{r}\right) = -\frac{g}{r^2}\cos\theta. \quad (14)$$

A. Colloid with angular-momentum conservation

The symmetric stress tensor for an incompressible AMC fluid can be expressed as

$$\boldsymbol{\sigma} = -P\mathbf{I} + \eta(\nabla\boldsymbol{v}^T + (\nabla\boldsymbol{v}^T)^T). \quad (15)$$

In spherical coordinates its components are

$$\sigma_{rr}(r) = -P + 2\eta\frac{\partial v_r}{\partial r}, \quad (16)$$

$$\sigma_{\theta r}(r) = \eta\left(\frac{1}{r}\frac{\partial v_r}{\partial\theta} - \frac{v_\theta}{r} + \frac{\partial v_\theta}{\partial r}\right), \quad (17)$$

which become

$$\sigma_{rr}(r) = -P_0 + 6a\eta g\cos\theta\frac{1}{r^2} - 12b\eta g\cos\theta\frac{1}{r^4}, \quad (18)$$

$$\sigma_{\theta r}(r) = -6b\eta g\sin\theta\frac{1}{r^4}, \quad (19)$$

with the velocity components of Eqs. (11) and (12), and the pressure of Eq. (10).

A particularly relevant quantity is the total force $\boldsymbol{\mathcal{S}}$ exerted on the colloid surface by the fluid,

$$\boldsymbol{\mathcal{S}} = \oint \boldsymbol{\sigma} \cdot d\boldsymbol{S}, \tag{20}$$

which reduces to

$$\mathcal{S} = \oint [\sigma_{rr}(R)\cos\theta - \sigma_{\theta r}(R)\sin\theta] dS \tag{21}$$

along the direction $\boldsymbol{g}$. The other components vanish due to symmetry. The direction of the surface element $d\boldsymbol{S}$ is along the outward normal of the particle surface, and $dS = R^2 \sin\theta\, d\theta d\phi$. The force $\mathcal{S}$ can be generally calculated in terms of Eqs. (18) and (19) to be

$$\mathcal{S} = 8\pi a \eta g. \tag{22}$$

1. Colloid exposed to an external force

Slip boundary condition: We first consider the case of a colloid with slip boundary conditions experiencing a constant external force and moving at velocity $\boldsymbol{u}$. A relevant example is a sedimenting colloidal sphere in a gravitational field. The flow field has to satisfy the two boundary conditions:

(1) Its normal component vanishes at the particle surface in the comoving reference frame. This implies that the component $v_r = \boldsymbol{v} \cdot \hat{\boldsymbol{r}}$ is equal to the velocity of the moving particle $v_r(R) = \boldsymbol{u} \cdot \hat{\boldsymbol{r}} = u\cos\theta$. Hence, with Eq. (11), we obtain

$$R^3 + 2aR^2 - 2b = 0. \tag{23}$$

(2) The slip boundary implies that the tangential stress vanishes at the particle surface, i.e., $\sigma_{\theta r}(R) = 0$, which, together with Eq. (19), yields $b = 0$ and $a = -R/2$. Thus, the resulting flow field is

$$\boldsymbol{v}(\boldsymbol{r}) = \frac{R}{2r}(\mathbf{I} + \hat{\boldsymbol{r}}\hat{\boldsymbol{r}}^T) \cdot \boldsymbol{u}. \tag{24}$$

This is a Stokeslet flow which decays with the inverse of the distance. The total force exerted on a colloid by the fluid moving at constant velocity $\boldsymbol{u}$ is the frictional force $\boldsymbol{F}_\gamma$. Substituting the value of a in Eq. (22), we get the well-known result [56]

$$F_\gamma = \mathcal{S} = -4\pi\eta R u \tag{25}$$

for the frictional force, which is opposite to the direction of particle motion.

No-slip boundary condition. For comparison, the velocity field around a no-slip particle is also provided. In this case, both, the normal and tangential components of the velocity field at the particle surface vanish in the particle reference frame, i.e., $\boldsymbol{v}(R) = \boldsymbol{u}$. In addition to Eq. (23), this implies $R^3 + aR^2 + b = 0$. Accordingly, the coefficients a and b are determined as $-3R^3/4$ and $-R^3/4$. Thus, we obtain the well-known expression of the velocity field [42]

$$\boldsymbol{v}(\boldsymbol{r}) = \frac{3R}{4r}(\mathbf{I} + \hat{\boldsymbol{r}}\hat{\boldsymbol{r}}^T) \cdot \boldsymbol{u} + \frac{R^3}{4r^3}(\mathbf{I} - 3\hat{\boldsymbol{r}}\hat{\boldsymbol{r}}^T) \cdot \boldsymbol{u}. \tag{26}$$

Comparing with Eq. (24), the velocity field around a sedimenting no-slip particle includes a source-dipole term. To obtain the hydrodynamic friction force, $a = -3R^3/4$ is inserted in Eq. (22), which results in the well-established relation (Stokes's law)

$$F_\gamma = -6\pi\eta R u. \tag{27}$$

2. Colloid in a phoretic field

Phoresis refers to the directional drift motion of a suspended particle in an inhomogeneous fluid environment [57]. Such inhomogeneities can be gradients of electric potentials (electrophoresis), concentration (diffusiophoresis), or temperature (thermophoresis). The phoretic force arises from the interaction of a large particle with an inhomogeneous surrounding fluid, hence it is an internal force in contrast to externally applied forces, like gravity, which are directly interacting with the colloid. It is therefore to be expected that the flow field induced by phoresis is different from that of a sedimenting colloid. Note that the phoretically induced velocity field is independent of the specific driving mechanism, since the governing equations and boundary conditions are the same for all mechanisms.

Freely moving phoretic particle. We first consider a phoretic colloidal particle drifting with velocity $\boldsymbol{u}$. The hydrodynamic boundary conditions in this case are the following:

(1) The normal component of the flow field vanishes in the particle reference frame. This corresponds to a colloid with slip boundary conditions and an external force; i.e., Eq. (23) also applies here.

(2) For a freely moving phoretic particle, the phoretic force balances the friction force. Hence, the integral of the stress tensor over the particle surface vanishes [15,57,58]. This means that $\mathcal{S} = 0$, which, together with Eq. (22), implies that $a = 0$, and with Eq. (23) $b = R^3/2$. The flow field in Eq. (9) around a freely moving phoretic colloidal sphere is then [15,57,58],

$$\boldsymbol{v}(\boldsymbol{r}) = \frac{R^3}{2r^3}(3\hat{\boldsymbol{r}}\hat{\boldsymbol{r}}^T - \boldsymbol{I}) \cdot \boldsymbol{u}. \tag{28}$$

This velocity field is a source dipole, decaying with respect to the distance to the center of the particle as $1/r^3$.

Fixed phoretic particle. When the particle is fixed by an externally applied force like a laser tweezer, the phoretic force $\boldsymbol{F}_P$ does not vanish due to the presence of the solvent inhomogeneity. Therefore, in response to the phoretic force, the surrounding fluid moves. Hence, the boundary conditions are the following:

(1) The normal component of the flow field vanishes at the particle surface in the laboratory reference frame, i.e, $v_r(R) = 0$. This condition, together with Eq. (11), implies that $aR^2 = b$.

(2) The fact that there is no motion in this case implies that the stress integrated over the particle surface corresponds to the phoretic force $\boldsymbol{\mathcal{S}} = \boldsymbol{F}_P$ [15,59,60]. Equation (22) can be then rewritten as

$$\mathcal{S} = 8\pi\eta F_P a, \tag{29}$$

which gives $a = 1/8\pi\eta$ and $b = R^2/8\pi\eta$. Insertion of a and b in Eq. (9) yields the velocity field [15,59,60],

$$\boldsymbol{v}(\boldsymbol{r}) = -\frac{1}{8\pi\eta r}(\hat{\boldsymbol{r}}\hat{\boldsymbol{r}}^T + \boldsymbol{I}) \cdot \boldsymbol{F}_P + \frac{R^2}{8\pi\eta r^3}(3\hat{\boldsymbol{r}}\hat{\boldsymbol{r}}^T - \boldsymbol{I}) \cdot \boldsymbol{F}_P. \tag{30}$$

The phoretic-force-induced field is a superposition of a Stokeslet and a source dipole, and it is therefore long ranged. This is in some aspects similar to a sedimenting particle with stick boundary conditions, except for the prefactor of the source-dipole term. In any case, the lack of motion and the fact that the driving force is internal renders them fundamentally different. It can straightforwardly be proven that the flow field Eq. (28) around a freely moving phoretic particle can be understood as that produced by a fixed phoretic object, as that in Eq. (30), superimposed with the flow field of a moving particle under an external force, as that in Eq. (24).

B. Colloid without angular-momentum conservation

In a mesoscopic solvent without angular momentum conservation, the stress tensor is nonsymmetric. However, the form of Stokes equations, specifically in the stationary state Eq. (8), is unaffected. Therefore, their general solution Eq. (9) is still valid. For no-slip boundaries, the stress tensor does not influence the flow field, as long as the Stokes equations are equal, since Eq. (20) can be written as

$$\oint \boldsymbol{\sigma} \cdot d\boldsymbol{S} = \int \nabla \cdot \boldsymbol{\sigma}\, dV \tag{31}$$

according to Gauss's theorem, where V is the volume inclosed by the surface S, and stress tensors differ by a term of vanishing divergence only. Hence, lack of AMC has no influence on the velocity field around a sedimenting particle with stick hydrodynamic boundaries, and the velocity field is given by Eq. (26). Accordingly, the friction is also not affected. However, this does not apply to slip boundaries.

We use the stress tensor of Eq. (4) for the MPC-SRD-a solvent. The extension to other mesoscopic methods without AMC would then follow the same procedure. Using spherical coordinates as in Sec. IV A, the relevant components of the stress tensor are

$$\sigma_{rr} = -P + (\hat{\eta} + \eta)\frac{\partial v_r}{\partial r}, \tag{32}$$

$$\sigma_{\theta r} = \hat{\eta}\left(\frac{1}{r}\frac{\partial v_r}{\partial \theta} - \frac{v_\theta}{r}\right) + \eta\frac{\partial v_\theta}{\partial r}, \tag{33}$$

which become

$$\sigma_{rr} = -P_0 + \frac{2a(\hat{\eta} + 2\eta)g\cos\theta}{R^2} - \frac{6b(\hat{\eta} + \eta)g\cos\theta}{R^4}, \tag{34}$$

$$\sigma_{\theta r} = (\hat{\eta} - \eta)\frac{ag\sin\theta}{R^2} - \frac{3bg(\hat{\eta} + \eta)\sin\theta}{R^4}, \tag{35}$$

with the pressure and velocity components of Eqs. (10)–(12). A calculation shows that the total force $\mathcal{S}$ in Eq. (21) is identical to Eq. (22).

1. Colloid exposed to an external force: Slip boundary condition

For comparison, we again consider a colloidal particle exposed to a constant external force moving with velocity $\boldsymbol{u}$. The boundary conditions are the same as in the case with AMC, namely, $v_r(R) = u\cos\theta$ and $\sigma_{\theta r}(R) = 0$. The first condition translates in Eq. (23), while the second condition implies

$$aR^2(\eta - \hat{\eta}) + 3b(\hat{\eta} + \eta) = 0. \tag{36}$$

Hence, we find

$$a = -\frac{3(\hat{\eta} + \eta)R}{4(\hat{\eta} + 2\eta)}, \quad b = \frac{(\eta - \hat{\eta})R^3}{4(\hat{\eta} + 2\eta)}. \tag{37}$$

Therefore, the velocity field of the fluid around a sedimenting colloidal sphere in terms of Eq. (9) becomes

$$\boldsymbol{v}(\boldsymbol{r}) = \frac{3(\hat{\eta} + \eta)R}{4(\hat{\eta} + 2\eta)r}(\boldsymbol{I} + \hat{\boldsymbol{r}}\hat{\boldsymbol{r}}^T)\cdot\boldsymbol{u} + \frac{(\eta - \hat{\eta})R^3}{4(\hat{\eta} + 2\eta)r^3}(3\hat{\boldsymbol{r}}\hat{\boldsymbol{r}}^T - \boldsymbol{I})\cdot\boldsymbol{u}, \tag{38}$$

which is clearly different from Eq. (24) for AMC. First, the prefactor of the Stokeslet term is different, and, more importantly, the source-dipole term is nonzero.

The hydrodynamic friction force is calculated using Eq. (22) together with Eq. (37),

$$F_\gamma = -6\pi\frac{\eta(\hat{\eta} + \eta)}{\hat{\eta} + 2\eta}Ru, \tag{39}$$

which can be rewritten as

$$F_\gamma = -4\pi\eta Ru\left[1 - \frac{\eta - \hat{\eta}}{2(\hat{\eta} + 2\eta)}\right]. \tag{40}$$

The first term in the brackets corresponds to the friction force of a sphere with slip boundary conditions in the presence of AMC. The second term leads to a reduced friction force in the absence of AMC. The effect will be largest for $\eta^k \ll \eta^c$, i.e., in the so-called collective regime where the solvent has liquid-like properties and a large Schmidt number [61]. Thus, the friction force is of the general form

$$F_\gamma = -C\pi\eta Ru, \tag{41}$$

with $C = 3$ for the viscosities of Eq. (6) (Pooley and Yeomans) and $C = 3.6$ for the viscosities of Eq. (5) (Ihle *et al.*), for $\eta^k = 0$. Hence, the different expressions for the stress tensor imply a significant difference in the frictional force which can be tested in simulations.

For the far-field fluid velocity, the source-dipole is negligible and Eq. (38) can be mapped to the velocity field with AMC in Eq. (24) by considering the hydrodynamic radius R_H instead of R.

2. Colloid in a phoretic field

As for an angular-momentum-conserving fluid, the hydrodynamic boundary conditions for a freely moving phoretic particle are $v_r(R) = u\cos\theta$ and $\boldsymbol{\mathcal{S}} = 0$, which implies that $a = 0$ and $b = R^3/2$. This is the same result as for a AMC fluid, and, consequently, the flow field is given by Eq. (28).

Moreover, the boundary conditions for a fixed phoretic particle are also identical with those for AMC, namely, $v_r(R) = 0$ and $\boldsymbol{\mathcal{S}} = \boldsymbol{F}_p$. This implies that $a = 1/8\pi\eta$ and $b = R^2/8\pi\eta$, and therefore the flow field is described by Eq. (30).

Thus, the absence of AMC does not modify the flow field produced by a phoretic particle, in contrast to the situation of an external force. This interesting result means that the hydrodynamic behavior of phoretic colloids can be correctly described by mesoscopic simulation methods without AMC,

which significantly simplifies the implementation of simulations. The reason behind this result is the fact that for a phoretic colloid the stress tensor enters only through the surface integral Eq. (20), which, as shown by the relation (31), is independent of the absence or presence of AMC.

C. Simulations of spherical colloids

In order to verify the previous analytical calculations, specifically the unexpected friction force with slip boundary conditions in the absence of AMC, we perform MPC-SRD-a and MPC-AT+a simulations, focusing on colloids experiencing an external force. The case of a phoretic colloidal particle has been investigated in a recent MPC-SRD-a simulation study [15]. The determined thermophoretically induced flow fields around spherical colloidal particles agree very satisfactorily with the predictions in Eqs. (28) and (30). This confirms the current theoretical prediction that no differences appear in the presence or absence of local AMC.

We consider a colloidal particle of radius $R = 4$ in a three-dimensional cubic box with periodic boundary conditions and size $L = 72$. Simulations are performed with an average of $\rho = 10$ particles per collision cell, the collision time step $h = 0.1$, and the rotation angle $\alpha = 120°$. These parameters yield the viscosity $\eta = 7.93$ according to the theoretical predictions [19,25,30,45,46,50,55], which is in close agreement with simulation results [62]. In case of MPC-AT+a, we use $h = 0.05$, for which simulations yield $\eta = 6.8$.

We consider the flow field $\tilde{\boldsymbol{v}}(\boldsymbol{r})$ in the vicinity of a fixed colloid with the velocity $\boldsymbol{u}_\infty$ at infinity. This is equivalent to the flow field $\boldsymbol{v}(\boldsymbol{r})$ around a colloidal particle moving with constant velocity $-\boldsymbol{u}_\infty$ driven by an external force in a quiescent fluid. The two flow fields are related by

$$\tilde{\boldsymbol{v}}(\boldsymbol{r}) = \boldsymbol{v}(\boldsymbol{r}) + \boldsymbol{u}_\infty. \tag{42}$$

The external flow along the z direction of the Cartesian reference frame is achieved by fixing the average velocity of the fluid in the plane perpendicular to the z axis farthest from the colloid center. The imposed fluid velocity is $\boldsymbol{u}_B = 0.004\hat{\boldsymbol{z}}$, where $\hat{\boldsymbol{z}}$ is the unit vector along the z axis. The corresponding Reynolds number $\mathrm{Re} = u_B R/\nu \sim 10^{-2}$ is low enough and the Stokes limit applies.

Figure 1 displays the velocity field around the fixed colloid obtained with the MPC-AT+a method. Due to symmetry, only a cross section of the flow field through the colloid center is presented. The flow pattern is qualitatively the same in the presence or absence of AMC. Visually, the two are hardly distinguishable. For a quantitative comparison, we need to determine the respective fluid velocities $\boldsymbol{u}_\infty$, which depend on lack or presence of AMC. Although the imposed boundary velocity is the same in both cases, $\tilde{\boldsymbol{v}}(L/2) = \boldsymbol{u}_B = 0.004\hat{\boldsymbol{z}}$, the corresponding asymptotic values $\boldsymbol{u}_\infty$ differ. For the MPC-AT+a solvent, Eqs. (24) and (42) yield $\boldsymbol{u}_\infty = (1 - 2R/L)^{-1}\boldsymbol{u}_B = 0.0045\hat{\boldsymbol{z}}$. For the MPC-SRD-a fluid, Eqs. (38) and (42) are employed, yielding to $\boldsymbol{u}_\infty = 0.0044\hat{\boldsymbol{z}}$.

The normalized simulation results with and without AMC are compared with the analytic predictions of Eqs. (24) and (38) in Fig. 2. The flow field is presented along the two representative axes parallel (∥) and perpendicular (⊥) to the external flow direction. Both axes intersect in the colloid center. Besides the statistical uncertainty, which is larger in the flow direction and for MPC-AT+a simulations, the agreement between the simulations and the analytical predictions is very satisfactory. This nicely supports the previous analytical scheme.

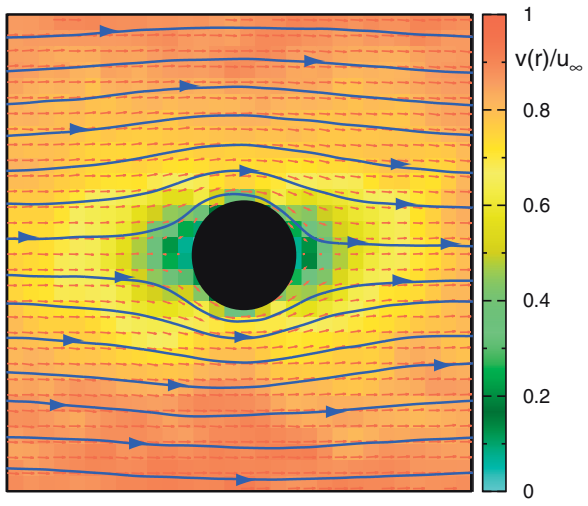

FIG. 1. (Color online) Velocity field of an externally applied fluid flow past a fixed colloidal sphere (cross section through the colloid center). Blue solid lines correspond to the stream lines, small red arrows are the solvent velocity field, and the background color code indicates the normalized velocity modulus.

The results in Fig. 2 show that the normalized flow field without AMC is always larger than that with AMC. This is consistent with the results in Eq. (40), where a reduced friction is expected in the absence of AMC. This means that the flow in the absence of AMC deviates less from the externally imposed flow, and can be intuitively understood as

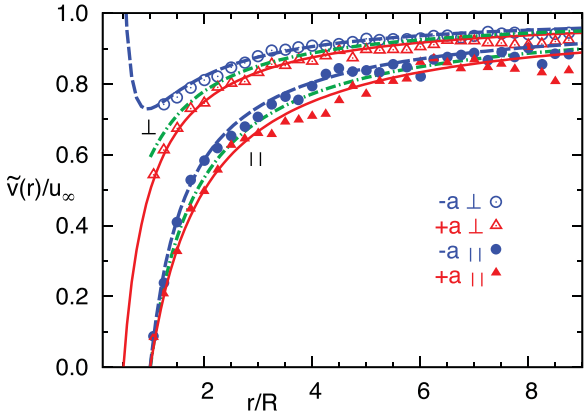

FIG. 2. (Color online) Normalized fluid velocity as a function of the separation from the center of a fixed colloidal particle in a fluid with a constant flow velocity at infinity. Symbols refer to the simulation results, with (+a, triangles) and without AMC (-a, circles), in an axis along the flow (∥, solid), and axis perpendicular to the flow (⊥, empty). Lines correspond to the analytical predictions. Discontinuous lines correspond to the case without AMC in Eq. (38) and solid lines to the AMC case in Eq. (24). Dashed lines account for the viscosities in Eq. (6) and dashed-dotted lines for that in Eq. (5).

TABLE I. Friction forces and friction coefficients for various MPC simulations, and the extracted coefficient C [cf. Eq. (41)]. The respective theoretical values for AMC and non-AMC simulations are $C = 3.1$ and $C = 4$ for the considered viscosities.

	F_γ	$\zeta = F_\gamma/u_\infty$	$C = \zeta/\pi\eta R$
MPC-SRD-a	1.265	290	2.91
MPC-AT+a	1.438	320	3.74

an additional resistance due to the conservation of angular momentum. The difference between the flow fields with and without AMC is largest at the colloid surface along the axis perpendicular to the flow field, where, for the parameters employed here, it can be as large as 35%. This difference disappears in the asymptotic limit of large distances.

The simulation results in Fig. 2 can be compared with theoretical predictions for the two existing expressions of the stress tensors [19,25]. For the employed parameters, the difference between the flows obtained with the viscosities Eqs. (6) and (5), respectively, is small. However, the simulation results show a better qualitative and quantitative agreement with the stress tensor of Pooley and Yeomans [25] and the viscosities of Eq. (6).

D. Friction coefficient

In addition, we determine the friction force of the colloid by calculating the total momentum exchange of the fluid particles with the colloid. The results are summarized in Table I. The related friction coefficient is obtained via $\zeta = F_\gamma/u_\infty$, where u_∞ is the flow velocity infinitely far from the fixed colloid, or equivalently, the colloid constant velocity in a quiescent fluid.

Within hydrodynamics, the friction coefficient can be analytically calculated as $\zeta = C\pi\eta R$ (Stokes's law). For the case of AMC, $C = 4$ as shown in Eqs. (25) and (40). In the absence of AMC, and for our specific values of η^k and η^c, $C = 3.1$ when accounting for the viscosity in Eq. (6), and $C = 3.6$ with the viscosity of Eq. (5).

The simulation results for C summarized in Table I underestimate the theoretical values (40) by approximately 7% for non-AMC fluids with the viscosity coefficients of Eq. (6), as well as for AMC fluids. In comparison, the value $C = 3.6$ with the viscosities of Eq. (5) is by about 24% larger than the simulation value. Hence, the simulation results show again a much better agreement with the stress tensor proposed by Pooley and Yeomans [25].

The discrepancy between the analytical and simulation results is not a finite-size effect, because we extrapolated to an infinite system by using u_∞ instead of u_B in $\zeta = F_\gamma/u_\infty$. The difference is a consequence of the fact that MPC, as a mesoscopic fluid model, does not capture hydrodynamics on short time and small length scales. The nonhydrodynamic friction on short time scales, known as Enskog friction due to uncorrelated collisions of fluid particles with the colloid, implies a smaller total friction coefficient [22,30,63]. However, the Enskog contribution becomes irrelevant with increasing colloidal radius [53]. Simulations of larger colloids verified this dependence, and we achieve an even better agreement between theoretical and simulation results.

Hence, we conclude that the friction coefficient of a slip sphere in a non-AMC solvent is $\zeta = 3\pi\eta R$ for $\eta^k \ll \eta^c$, in contrast to that in an AMC solvent, which is $\zeta = 4\pi\eta R$. This reduction of the friction coefficient by 25% noticeably affects several related quantities, such as the mobility, the diffusion coefficient, and the hydrodynamic radius. Therefore, special attention has to be paid to the interpretation of simulation results measured by MPC-a methods. For example, in simulations of thermophoretic colloids embedded in a non-AMC fluid [15], there exists a small difference in the thermal diffusion factor obtained by directly measuring the thermal force exerted on a fixed colloid, and by measuring the thermophoretic velocity of a moving particle. By considering the diminished friction coefficient the observed difference can be explained.

V. CIRCULAR COUETTE FLOW

In order to find the correct stress tensor for a MPC-a fluid, we also evaluate the velocity field for a circular Couette flow. Since the stress tensor enters here explicitly via the boundary condition, this will permit us to clearly distinguish between the two proposed expressions. For the Couette flow, we consider two concentric cylinders of radius R_1 and R_2 (see Fig. 3). The outer cylinder rotates at constant angular velocity ω, and we assume no-slip boundary conditions, while the inner cylinder has slip boundary conditions.

Given the symmetry of the problem, cylindrical coordinates (r,θ,z) are the appropriate choice, and the fluid velocity can be expressed as $\boldsymbol{v}(r,\theta,z) = v_\theta(r)\hat{\boldsymbol{\theta}}$. The fluid dynamical equations in the Stokes limit in Eqs. (7) and (4) can be solved by a constant pressure and

$$v_\theta(r) = Ar + B/r, \tag{43}$$

where the parameters A and B are determined by the boundary conditions. The no-slip boundary at the outer wall implies

$$v_\theta(R_2) = R_2\omega, \tag{44}$$

while the slip boundary condition on the inner wall requires

$$\sigma_{zr}(R_1,\theta,z) = 0, \tag{45}$$

$$\sigma_{\theta r}(R_1,\theta,z) = 0. \tag{46}$$

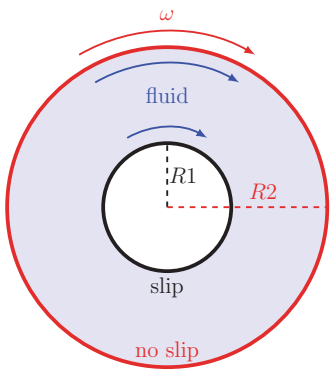

FIG. 3. (Color online) Sketch of circular Couette flow between concentric cylinders.

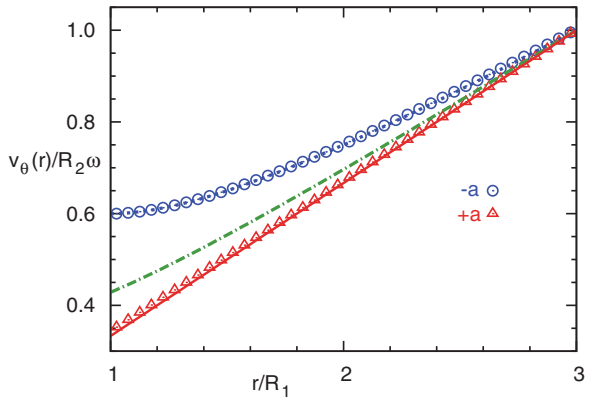

FIG. 4. (Color online) Couette-flow velocity in θ direction as a function of the normalized distance from the cylinder axis. Symbols correspond to the simulation results with AMC (triangles) and without AMC (circles). Lines correspond to the analytical predictions. Similar to Fig. 2, the dashed line accounts for the case without AMC and viscosities in Eq. (6), the dashed-dotted line for the case without AMC and viscosities in Eq. (5), and the solid line to the AMC case.

Note that $\sigma_{zr} = 0$ is automatically fulfilled by our ansatz and $\sigma_{\theta r}$ can be determined by Eq. (33). This yields

$$A = \frac{\omega x}{1+x}, \quad B = \frac{\omega R_2^2}{1+x}, \quad x = \frac{R_2^2}{R_1^2}\frac{\eta+\hat{\eta}}{\eta-\hat{\eta}}. \tag{47}$$

Interestingly, in the MPC liquid-like limit, where $\eta^k \ll \eta^c$, the coefficient x is independent of the viscosity and is only a function of the ratio of the radii R_1 and R_2. The ratio itself depends on the particular stress tensor. We find $x = R_2^2/R_1^2$ for the coefficients in Eq. (6) and $x = 3R_2^2/R_1^2$ for the coefficients in Eq. (5). This clearly reflects a difference in the flow fields of the two stress tensors.

In the case of angular momentum conserving fluids, $\eta = \hat{\eta}$ and a uniformly rotating flow does not produce any stresses in an AMC fluid, such that $v_\theta(r) = \omega r$. As Eq. (47) for $\eta \neq \hat{\eta}$ reveals, this is intrinsically different in the absence of AMC, where the fluid flow is noticeably affected.

To verify these results, we perform simulations with and without AMC. Thereby, we apply the MPC-SRD-a and MPC-SRD+a approach [45,52] with the Maxwell-Boltzmann-scaling (MBS) thermostat [21,62]. The MPC fluid is confined between cylinders of radius $R_1 = 10$ and $R_2 = 30$, both of length $L_z = 40$, and periodic boundary conditions are applied along the z direction. The angular velocity of the outer cylinder is fixed at $\omega = 0.003$, the MPC rotation angle is chosen as $\alpha = 130^\circ$, and the particle density as $\rho = 10$. For MPC-SRD-a, the collision time is $h = 0.01$, and for MPC-SRD+a it is $h = 0.0043$, which yields in both cases $\eta = 82$ as established by the kinetic theory [19] for the $-a$ fluid, and by independent simulations for the $+a$ fluid. Given the linear velocity of the outer cylinder $R_2\omega$, the Reynolds number is Re $\simeq 0.1$, and the flow velocity can be described within Stokes limit.

Results for the flow velocities $v_\theta(r)$ are presented in Fig. 4. We find a major difference between the non-AMC and AMC fluids. For non-AMC fluids, the simulation results agree very well with the theoretical predictions based on the stress tensor in Eq. (4) with the viscosities in Eq. (6). As discussed above, for an AMC fluid, the velocity profile is linear and independent of viscosity.

VI. CONCLUSIONS

We have investigated the influence of angular momentum conservation on the flow field in the vicinity of a hard-sphere colloidal particle by analytical theory and mesoscale hydrodynamic simulations. Colloids in external force fields and in phoretic fields have been considered. To determine in which circumstances angular momentum conservation plays a role, and to quantify this effect, is of fundamental importance for the proper interpretation of obtained simulation results.

Qualitatively the flow fields are the same in the presence and absence of angular momentum conservation. Moreover, they are identical in the case of no-slip boundaries, and interestingly also in the case of colloids in a phoretic field. Pronounced differences are obtained for colloids with slip boundary conditions exposed to an external force. A smaller friction coefficient is found in systems without locally conserved angular momentum compared to those where such conservation is fulfilled; i.e., Stokes's law is different with and without AMC. Nevertheless, dilute colloid solutions are expected to exhibit the same behaviors in the coarse-grained fluid with and without AMC, because their far-field velocities can be mapped onto each other by just considering different effective hydrodynamic radii.

In addition, we confirmed that boundary conditions (slip vs no-slip) determine the flow profile. In particular, we have illustrated the differences in the Couette-flow flow profiles for two stress tensors suggested for MPC systems. Thereby, we have demonstrated that the expression provided by Pooley and Yeomans [25] provides quantitative agreement with simulations.

Our studies clarify various aspects of lack of AMC on the dynamics of colloids. Yet they underline the power of the mesoscopic approaches in simulations of soft matter systems.

ACKNOWLEDGMENT

M.Y. gratefully acknowledges support from National Natural Science Foundation of China (Grant No. 11404379).

[1] J. K. G. Dhont, *An Introduction to Dynamics of Colloids* (Elsevier, Amsterdam, 1996).
[2] W. Russel, D. Saville, and W. Schowalter, *Colloidal Dispersions* (Cambridge University Press, Cambridge, 1995).
[3] S. Succi, *The Lattice Boltzmann Equation: For Fluid Dynamics and Beyond* (Clarendon, Oxford, 2001).
[4] G. A. Bird, *Molecular Gas Dynamics* (Clarendon, Oxford, 1976).
[5] F. J. Alexander and A. L. Garcia, Comp. Phys. **11**, 588 (1997).
[6] P. J. Hoogerbrugge and J. M. V. A. Koelman, Europhys. Lett. **19**, 155 (1992).
[7] P. Espanol and P. B. Warren, Europhys. Lett. **30**, 191 (1995).

[8] C. P. Lowe, Europhys. Lett. **47**, 145 (1999).
[9] A. Malevanets and R. Kapral, J. Chem. Phys. **110**, 8605 (1999).
[10] R. Kapral, Adv. Chem. Phys. **140**, 89 (2008).
[11] G. Gompper, T. Ihle, D. M. Kroll, and R. G. Winkler, Adv. Polym. Sci. **221**, 1 (2009).
[12] U. Frisch, B. Hasslacher, and Y. Pomeau, Phys. Rev. Lett. **56**, 1505 (1986).
[13] D. Lüsebrink and M. Ripoll, J. Chem. Phys. **136**, 084106 (2012).
[14] D. Lüsebrink, M. Yang, and M. Ripoll, J. Phys.: Condens. Matter **24**, 284132 (2012).
[15] M. Yang and M. Ripoll, Soft Matter **9**, 4661 (2013).
[16] C. Junghans, M. Praprotnik, and K. Kremer, Soft Matter **4**, 156 (2008).
[17] P. Español and M. Revenga, Phys. Rev. E **67**, 026705 (2003).
[18] K. Müller, D. A. Fedosov, and G. Gompper, J. Comput. Phys. **281**, 301 (2015).
[19] T. Ihle, E. Tüzel, and D. M. Kroll, Phys. Rev. E **72**, 046707 (2005).
[20] E. Tüzel, T. Ihle, and D. M. Kroll, Phys. Rev. E **74**, 056702 (2006).
[21] C. Huang, A. Chatterji, G. Sutmann, G. Gompper, and R. G. Winkler, J. Comput. Phys. **229**, 168 (2010).
[22] J. T. Padding and A. A. Louis, Phys. Rev. E **74**, 031402 (2006).
[23] G. K. Batchelor, *An Introduction to Fluid Dynamics* (Cambridge University Press, Cambridge, 1967).
[24] J. F. Ryder, *Mesoscopic Simulations of Complex Fluids*, Ph.D. thesis, University of Oxford, 2005.
[25] C. M. Pooley and J. M. Yeomans, J. Phys. Chem. B **109**, 6505 (2005).
[26] I. O. Götze, H. Noguchi, and G. Gompper, Phys. Rev. E **76**, 046705 (2007).
[27] M. Yang and M. Ripoll, Soft Matter **10**, 1006 (2014).
[28] M. Yang, R. Liu, M. Ripoll, and K. Chen, Nanoscale **6**, 13550 (2014).
[29] M. Yang, M. Ripoll, and K. Chen, J. Chem. Phys. **142**, 054902 (2015).
[30] A. Malevanets and R. Kapral, J. Chem. Phys. **112**, 7260 (2000).
[31] M. Hecht, J. Harting, T. Ihle, and H. J. Herrmann, Phys. Rev. E **72**, 011408 (2005).
[32] J. T. Padding and A. A. Louis, Phys. Rev. Lett. **93**, 220601 (2004).
[33] G. Rückner and R. Kapral, Phys. Rev. Lett. **98**, 150603 (2007).
[34] A. Wysocki, C. P. Royall, R. G. Winkler, G. Gompper, H. Tanaka, A. van Blaaderen, and H. Löwen, Soft Matter **5**, 1340 (2009).
[35] A. Moncho-Jordá, A. A. Louis, and J. T. Padding, Phys. Rev. Lett. **104**, 068301 (2010).
[36] M. Yang and M. Ripoll, Phys. Rev. E **84**, 061401 (2011).
[37] K. Milinković, J. T. Padding, and M. Dijkstra, Soft Matter **7**, 11177 (2011).
[38] S. Thakur and R. Kapral, Phys. Rev. E **85**, 026121 (2012).
[39] A. Moncho-Jordá, A. A. Louis, and J. T. Padding, J. Chem. Phys. **136**, 064517 (2012).
[40] J. T. Padding, A. Wysocki, H. Löwen, and A. A. Louis, J. Phys.: Condens. Matter **17**, S3393 (2005).
[41] M. Yang, A. Wysocki, and M. Ripoll, Soft Matter **10**, 6208 (2014).
[42] L. D. Landau and E. M. Lifshitz, *Fluid Mechanics* (Pergamon Press, Oxford, 1959).
[43] R. Golestanian, Phys. Rev. Lett. **102**, 188305 (2009).
[44] M. N. Popescu, S. Dietrich, M. Tasinkevych, and J. Ralston, Eur. Phys. J. E **31**, 351 (2010).
[45] H. Noguchi and G. Gompper, Phys. Rev. E **78**, 016706 (2008).
[46] T. Ihle and D. M. Kroll, Phys. Rev. E **63**, 020201(R) (2001).
[47] E. Allahyarov and G. Gompper, Phys. Rev. E **66**, 036702 (2002).
[48] A. Lamura, G. Gompper, T. Ihle, and D. M. Kroll, Europhys. Lett. **56**, 319 (2001).
[49] A. Lamura and G. Gompper, Eur. Phys. J. E **9**, 477 (2002).
[50] R. G. Winkler and C.-C. Huang, J. Chem. Phys. **130**, 074907 (2009).
[51] C.-C. Huang, G. Gompper, and R. G. Winkler, Phys. Rev. E **86**, 056711 (2012).
[52] M. Theers and R. G. Winkler, Soft Matter **10**, 5894 (2014).
[53] M. Theers and R. G. Winkler, Phys. Rev. E **91**, 033309 (2015).
[54] T. Ihle, Phys. Chem. Chem. Phys. **11**, 9667 (2009).
[55] N. Kikuchi, C. M. Pooley, J. F. Ryder, and J. M. Yeomans, J. Chem. Phys. **119**, 6388 (2003).
[56] J. P. Hansen and I. Mc Donald, *Theory of Simple Liquids* (Academic, New York, 1986).
[57] J. L. Anderson, Annu. Rev. Fluid Mech. **21**, 61 (1989).
[58] A. Würger, Phys. Rev. Lett. **98**, 138301 (2007).
[59] R. D. Leonardo, F. Ianni, and G. Ruocco, Langmuir **25**, 4247 (2009).
[60] J. Morthomas and A. Würger, Phys. Rev. E **81**, 051405 (2010).
[61] M. Ripoll, K. Mussawisade, R. G. Winkler, and G. Gompper, Phys. Rev. E **72**, 016701 (2005).
[62] C.-C. Huang, A. Varghese, G. Gompper, and R. G. Winkler, Phys. Rev. E **91**, 013310 (2015).
[63] J. K. Whitmer and E. Luijten, J. Phys.: Condens. Matter **22**, 104106 (2010).